The Astrophysical Journal, 957:42 (6pp), 2023 November 1 https://doi.org/10.3847/1538-4357/acf9f4

Simultaneous Observation of the Inner and Outer Electron Diffusion Region in Reconnection with Large Guide Field

Z. C. Tian[1,2], M. Zhou[1,2], H. Y. Man[2], Z. H. Zhong[1,2], X. H. Deng[2], D. J. Gershman[3], Y. V. Khotyaintsev[4], and C. T. Russell[5]
[1] School of Physics and Materials Science, Nanchang University, Nanchang 330031, People's Republic of China; monmentum82@gmail.com
[2] Institute of Space Science and Technology, Nanchang University, Nanchang 330031, People's Republic of China
[3] NASA Goddard Space Flight Center, Greenbelt, MD, USA
[4] Swedish Institute of Space Physics, Uppsala, Sweden
[5] University of California, Los Angeles, Los Angeles, CA, USA
Received 2023 June 5; revised 2023 August 23; accepted 2023 September 13; published 2023 October 26

Abstract

This paper presents a simultaneous observation of the inner and outer electron diffusion region (EDR) at the dayside magnetopause by the magnetospheric multiscale (MMS) spacecraft. The EDR was observed in magnetic reconnection with a large guide field. The inner EDR was characterized by positive $\boldsymbol{J}\cdot\boldsymbol{E}'$ while the outer EDR is manifested by negative $\boldsymbol{J}\cdot\boldsymbol{E}'$ and opposite out-of-plane electric field to that in the inner EDR. One pair of the spacecraft detected the inner EDR while the other pair encountered the outer EDR. Moreover, the two pairs were on the opposite side of the X-line as they observed the bidirectional accelerated electron jets. The fortuitous formation of MMS allows us to estimate the maximum length of the inner EDR as $\sim 36\, d_e$ and the lower bound of the reconnection rate as 0.142 ± 0.041. These observations have far-reaching implications for understanding the electron physics in reconnection.

Unified Astronomy Thesaurus concepts: Magnetic fields (994); Solar magnetic reconnection (1504); Plasma astrophysics (1261); Plasma physics (2089); Space plasmas (1544)

1. Introduction

Magnetic reconnection is an important energy conversion mechanism responsible for many explosive phenomena in our solar-terrestrial system, such as solar flares, magnetospheric storms, etc. (Priest & Forbes 2000; Deng & Matsumoto 2001; Lin et al. 2005). The electron diffusion region (EDR) is the crucial region of magnetic reconnection, in which the dissipation mechanism causes magnetic field lines to break and reconnect. Electron physics in the EDR determines the initiation and progression of reconnection (Vasyliunas 1975; Burch et al. 2016; Zhou et al. 2022). In the EDR, electrons are decoupled from magnetic field lines ($\boldsymbol{E}+\boldsymbol{V_e}\times\boldsymbol{B}\neq 0$) and accelerated by the reconnection electric field, forming a strong out-of-plane current and the bidirectional electron outflow with a speed exceeding the ion-Alfvén speed (Phan et al. 2018; Torbert et al. 2018; Zhou et al. 2019).

The EDR develops a two-scale structure along the outflow direction: the outer EDR and the inner EDR (Daughton et al. 2006; Fujimoto 2006; Karimabadi et al. 2007; Shay et al. 2007). The inner EDR is confined at the X-line while the outer EDR can extend far away (a few to tens of ion inertial lengths) from the X-line (Phan et al. 2007). Electrons are accelerated in the inner EDR, which corresponds to a positive energy dissipation $\boldsymbol{J}\cdot\boldsymbol{E}'=\boldsymbol{J}\cdot(\boldsymbol{E}+\boldsymbol{V_e}\times\boldsymbol{B})>0$ (Torbert et al. 2018; Zhou et al. 2019). The outer EDR has a negative energy dissipation $\boldsymbol{J}\cdot\boldsymbol{E}'<0$, hence electrons are decelerated and lose energy in the outer EDR (Zenitani et al. 2011; Le et al. 2013; Hwang et al. 2017). The outer EDR does not control the reconnection rate since the electron inflow does not go through the outer EDR (Karimabadi et al. 2013). A recent study by Zhong et al. (2022) illustrates that the EDR also develops multiple fine structures along the inflow direction, which is caused by the oblique tearing instability during the 3D evolution of reconnection (Liu et al. 2013).

The aspect ratio of the inner EDR is intimately related to the reconnection rate, which is one of the most important parameters of reconnection (e.g., Liu et al. 2017). In general, the dimensionless reconnection rate can be approximated as δ/L, where δ and L are the thickness (along the inflow direction) and length (along the outflow direction) of the inner EDR, respectively. This ratio has rarely been determined experimentally, particularly because it is difficult to evaluate the EDR length L. Torbert et al. (2018) estimate the EDR length as (12–17) electron inertial lengths by using the four-spacecraft timing analysis of the reconnected magnetic field component B_N. Here we present a unique reconnection event at the magnetopause. The magnetospheric multiscale (MMS) tetrahedron fortunately circumscribed the reconnection X-line and observed both the outer and inner EDR simultaneously in this event. Based on this particular spacecraft geometry around the X-line, we estimate the maximum length of the inner EDR and the minimum reconnection rate of this event.

2. Event Overview

MMS spacecraft provided the data for this study, including the 3D magnetic field vectors from the fluxgate magnetometer instrument (Russell et al. 2016), 3D electric field vectors from the electric double probe instruments (Ergun et al. 2016; Lindqvist et al. 2016), and 3D plasma moments from the fast plasma investigation instruments (Pollock et al. 2016).

Figure 1 shows the overview of MMS observations from 22:00 UT to 22:25 UT on 2016 January 7, when the MMS was

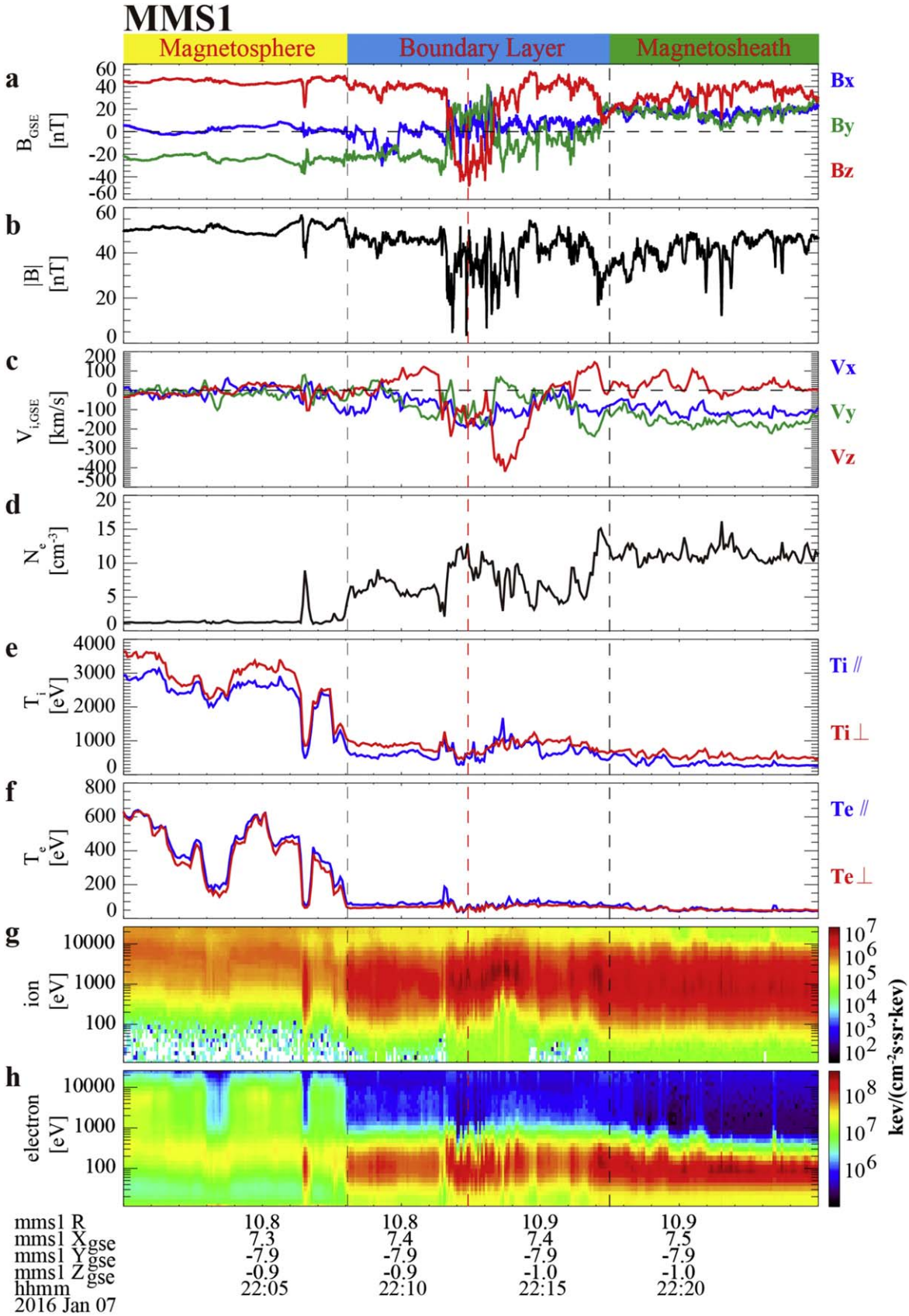

Figure 1. Overview of MMS1 observations from 22:00 to 22:25 UT on 2016 January 7. (a) The three components of magnetic fields; (b) the magnitude of the magnetic field; (c) the three components of the ion bulk velocity; (d) electron number density; (e) ion and (f) electron parallel (blue) and perpendicular (red) temperatures; (g) ion and (h) electron differential energy fluxes. The red dashed line marks the secondary reconnection event studied in this paper. The vectors are displayed in GSE coordinates.

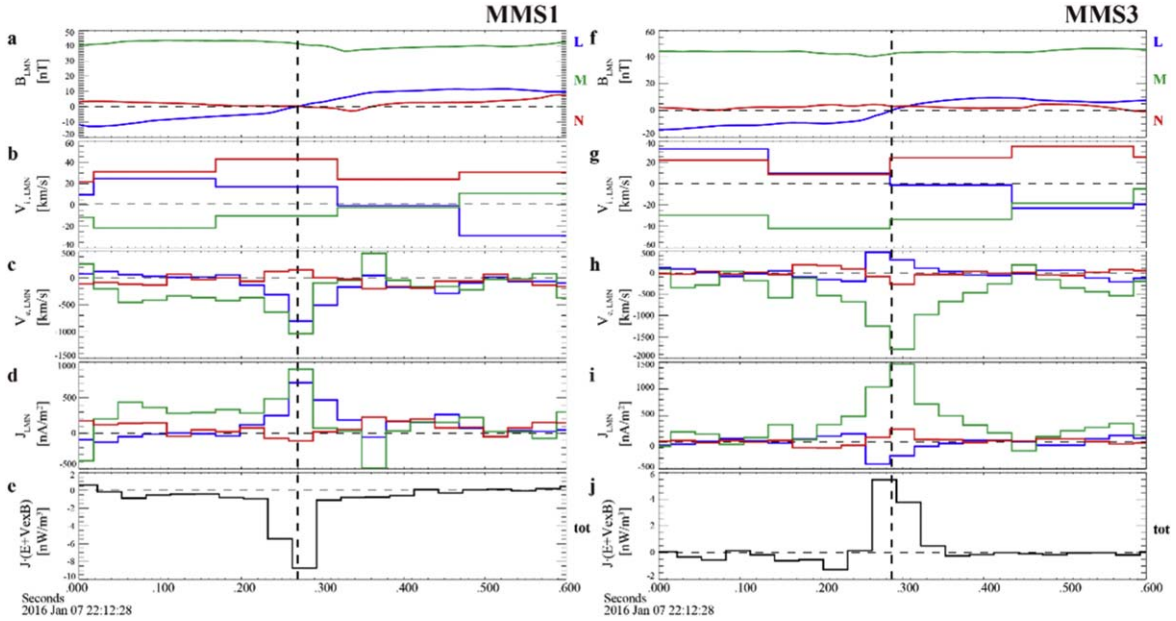

Figure 2. Detailed observations of the secondary reconnection by MMS1 (left column) and MMS3 (right column). (a) and (f) magnetic field; (b) and (g) ion bulk velocity; (c) and (h) electron bulk velocity; (d) and (i) electric current density calculated by plasma density and velocity; (e) and (j) energy dissipation $\boldsymbol{J}\cdot\boldsymbol{E}'=\boldsymbol{J}\cdot(\boldsymbol{E}+\boldsymbol{V}_e\times\boldsymbol{B})$. All the vectors are displayed in the LMN coordinate system. The background ion flow velocity has been subtracted from the ion and electron bulk velocity.

around [7.4, −7.9, −1.0] R_E (R_E is the Earth's radius) in the Geocentric Solar Ecliptic (GSE) coordinates. Four MMS spacecraft formed a regular tetrahedron in space with an average spacing of ∼44 km. MMS was in the magnetosphere proper before 22:08 UT except around 22:07:30 UT when MMS crossed into the magnetopause boundary layer and quickly moved back to the magnetosphere as shown in Figures 1(c)–(f). The magnetic field in the magnetosphere is relatively stable and mainly points northward (positive B_z) and dawnward (negative B_y).

The boundary layer was filled with mixed populations from the magnetosphere and magnetosheath (Figures 1(g)–(h)). The magnetic field B_z changes sign from positive to negative and returns back to positive in the boundary layer, accompanied by a change of the interplanetary magnetic field B_z from negative to positive after 22:10 UT (not shown). The fluctuations of magnetic fields are larger in the boundary layer than in the magnetosphere. MMS recorded a fast ion bulk flow with a peak speed of about 400 km s^{-1} in the $-\boldsymbol{Z}$ direction in the boundary layer (Figure 1(c)) and the ion flow in all three directions is approximately 200 km s^{-1} around the secondary reconnection we studied, denoted by a dashed red line (22:12:28 UT). These findings indicate that the MMS was positioned within a rapidly flowing turbulent environment and the secondary reconnection we studied was within the outflow region of a large-scale magnetopause reconnection.

3. Observations of the Secondary Reconnection

The red dashed line in Figure 1 marks a secondary reconnection site within the exhaust. Figure 2 details the observations of this secondary reconnection by MMS1 and MMS3. All the vectors are presented in the local boundary normal (LMN) coordinate system, with the transformation from Geocentric Solar Magnetospheric coordinates to LMN given by $\boldsymbol{L}=$ [0.935, 0.171, 0.308] pointing to the reconnecting magnetic component, $\boldsymbol{N}=$ [−0.312, 0.810, 0.496], pointing to the normal of the current sheet, and $\boldsymbol{M}=$ [0.165, 0.560, −0.812] completing a right-handed orthogonal coordinate system. The normal direction $\boldsymbol{N}$ is determined through the timing analysis based on the profile of the magnetic field B_x (Russell et al. 1983). We find $\boldsymbol{L}'$ as the maximum variation direction of the minimum variance analysis of magnetic fields (Sonnerup et al. 1998). Then, we obtain $\boldsymbol{M}$ by $\boldsymbol{M}=\boldsymbol{N}\times\boldsymbol{L}'$, and use $\boldsymbol{M}$ and $\boldsymbol{N}$ to find $\boldsymbol{L}$: $\boldsymbol{L}=\boldsymbol{M}\times\boldsymbol{N}$.

MMS detected the reversal of the magnetic field B_L from negative to positive around 22:12:28.3 UT (observations of MMS2 and MMS4 are shown in Figure 3), corresponding to an intense out-of-plane current J_M with a peak density of 900 nA m^{-2} observed by MMS1 and 1500 nA m^{-2} seen by MMS3. This out-of-plane current was primarily contributed by electrons as electron bulk speed $v_{eM}\sim-$(1000–2000 km s^{-1}) and is about 1 order of magnitude larger than the ion bulk speed $v_{iM}\sim 100$ km s^{-1}. Around the B_L reversal, MMS1 detected an electron jet in the $-\boldsymbol{L}$ direction with a peak speed of about 800 km s^{-1}, while MMS3 detected an electron jet in the $+\boldsymbol{L}$ direction with a peak speed of about 500 km s^{-1}. Since this current sheet was embedded within a large-scale southward flow, the background flow speed has been subtracted from both the ion and electron bulk speed. The observed bidirectional electron jet suggests that there is an active X-line between MMS1 and MMS3 in the $\boldsymbol{L}$ direction (e.g., Phan et al. 2018). We choose the maximum value of $|B_L|$ in the immediate vicinity of $B_L=0$ on both sides of the current sheet to locate the inflow region. The inflow magnetic field B_L is $-14.8\,nT$ and $11.9\,nT$, respectively. The plasma density and temperature changes from 4.2 and 5.0 cm^{-3} and 760 to 680 eV across the current sheet (not shown). Therefore, we suggest that MMS detected a reconnecting current sheet with a weak asymmetry. Note that there is a uniform guide field of $B_g\sim 41\,nT\sim 3.2\,B_0$ in the reconnection layer, where B_0 is the asymptotic magnetic field in the $\boldsymbol{L}$ direction. The electron jet speeds are much larger than the hybrid inflow ion-Alfvén speed of ∼170 km s^{-1},

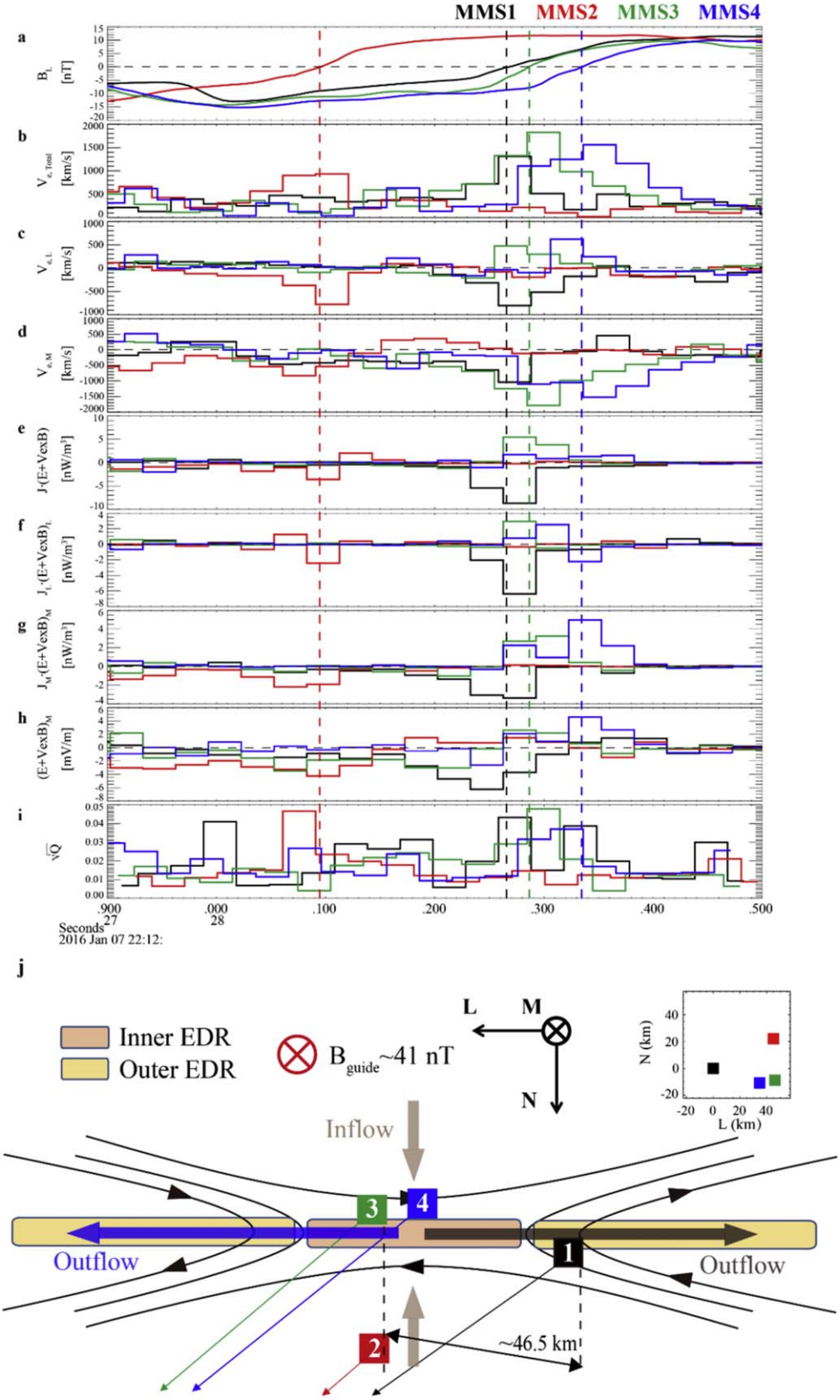

Figure 3. Successive observation of the inner and outer EDR by the four MMS spacecraft. (a) $\boldsymbol{L}$ component of magnetic field; (b) the magnitude of the electron bulk velocity; (c) $\boldsymbol{L}$ and (d) $\boldsymbol{M}$ component of the electron bulk velocity; (e) $\boldsymbol{J} \cdot \boldsymbol{E}'$; (f) $J_L E'_L$; (g) $J_M E'_M$; (h) E'_M; (i) the degree of electron nongyrotropy $\sqrt{Q}$; (j) schematic view of this reconnection layer and the spacecraft trajectory in the L–N plane.

indicating that the spacecraft were very close to the X-line. Interestingly, we find that the variation of v_{iL} is significantly smaller than v_{eL} and the inflow ion-Alfvén speed. The absence of the obvious ion outflow may be due to the spacecraft being too close to the X-line where the ion bulk flow is not fully developed.

Employing the spatiotemporal difference method (Shi et al. 2006), we find that the speed of the current sheet in the $\boldsymbol{N}$ direction is about 120 km s^{-1}, while the timing analysis yields a normal speed of ~150 km s^{-1}. Since MMS crossed the current sheet in less than 0.15 s, the corresponding current sheet thickness is less than 150 km s^{-1} × 0.15 s ~ 9 de, where $d_e \sim 2.6$ km is the electron inertial length in the inflow region. The electron-scale current sheet was not inside a much thicker ion-scale current sheet.

4. Observations of the Outer and Inner EDR

MMS3 detected a large positive energy dissipation $\boldsymbol{J}\cdot\boldsymbol{E}' = \boldsymbol{J}\cdot(\boldsymbol{E}+\boldsymbol{V_e}\times\boldsymbol{B})$ up to $6\,nW/m^3$, whereas $\boldsymbol{J}\cdot\boldsymbol{E}'$ measured by MMS1 was negative with a peak value around -8 nW/m^3, suggesting the conversion of plasma energy to magnetic energy. Figure 3 contrasts the four spacecraft observations around this reconnecting current sheet. It is shown that the four MMS spacecraft successively crossed the current sheet following the sequence of MMS2, MMS1, MMS3, and MMS4. The relative position and trajectories of the four spacecraft across the reconnection layer in the $\boldsymbol{L}-\boldsymbol{N}$ plane are sketched in Figure 3(j). All four spacecraft observed the enhancement of the electron bulk speed in the $\boldsymbol{L}$ and $\boldsymbol{M}$ directions. The opposite outflow in the $\boldsymbol{L}$ direction detected by MMS indicates that MMS1 and MMS2 were on the $-\boldsymbol{L}$ side of the X-line, while MMS3 and MMS4 were on the $+\boldsymbol{L}$ side of the X-line.

Nongyrotropic electrons were observed in this thin layer by all four spacecraft, manifested by the enhancement of the nongyrotropy parameter $\sqrt{Q}$ up to 0.05. $\sqrt{Q}$ is defined as $\sqrt{1-\frac{4I_2}{(I_1-P_{\parallel})(I_1+3P_{\parallel})}}$, where $I_1 = P_{xx}+P_{yy}+P_{zz}$, $I_2 = P_{xx}P_{yy}+P_{xx}P_{zz}+P_{yy}P_{zz}-(P_{xy}P_{yx}+P_{xz}P_{zx}+P_{yz}P_{zy})$ and $P_{\parallel}$ is the parallel pressure (Swisdak 2016). Other parameters to identify the EDR as proposed by Scudder et al. (2015) have also been examined, such as the electron Mach number $M_{e\perp}$, electron energy gain per cyclotron period ϵ_e, and the relative strength of the electric and magnetic force in the bulk electron rest frame δ_e. They all peaked coincident with $\sqrt{Q}$ (not shown). Although these signatures are not uniquely associated with the EDR, they support that all four spacecraft crossed the EDR. MMS3/MMS4 captured the inner EDR with positive energy dissipation ($\boldsymbol{J}\cdot\boldsymbol{E}' > 0$) and positive nonideal electric field ($E'_M > 0$), i.e., the out-of-plane reconnection electric field, while MMS1/MMS2 encountered the outer EDR, the distinct feature of which is the negative energy dissipation ($\boldsymbol{J}\cdot\boldsymbol{E}' < 0$) and the opposite out-of-plane electric field to the reconnection electric field ($E'_M < 0$) (Zenitani et al. 2011; Hwang et al. 2017).

$\boldsymbol{J}\cdot\boldsymbol{E}'$ observed by the four spacecraft are mainly contributed by $J_L E'_L$ and $J_M E'_M$. They are negative as observed by MMS1, suggesting that the electron outflow is slowed down in both the $\boldsymbol{L}$ and $\boldsymbol{M}$ directions. MMS3 observed positive $J_L E'_L$ and $J_M E'_M$ while $J_M E'_M$ is positive, and $J_L E'_L$ changes from positive to negative as observed by MMS4.

5. Reconnection Rate

A unique feature of this event is that MMS1/MMS2 and MMS3/MMS4 were on the opposite side of the X-line. Notably, MMS1 was situated in the outer EDR and MMS3 was situated in the inner EDR, hence the maximum length of the inner EDR must be smaller than the distance between MMS1 and MMS3, which is about 46.5 km. Note that this distance is a rotation invariant and thus is independent to coordinate transformation. Therefore, the maximum length of the inner EDR is $L \approx 2\times 46.5$ km $= 93$ km $\sim 36\ d_e$.

We employed a Gaussian fitting to the observed total current density observed by MMS3 and MMS4, which crossed the inner EDR. The obtained duration of the inner EDR is 0.078 and 0.114 s, respectively. Therefore, the thickness of the inner EDR was estimated as (120 ~ 150 km s^{-1}) × (0.078 s ~ 0.114 s) = 13.2 ± 3.8 km, and the corresponding minimum dimensionless reconnection rate is estimated as $R \sim \frac{\delta}{L} \sim (13.2\pm 3.8\ \text{km})/93\ \text{km} = 0.142\pm 0.041$, which is consistent with the value of fast reconnection in previous studies (Xiao et al. 2007; Chen et al. 2017; Liu et al. 2017; Zhong et al. 2020).

6. Discussion and Summary

From Figure 3 one can see that the total electron bulk speed observed by MMS3 and MMS4 is larger than that observed by MMS1 and MMS2. This is consistent with the scenario that electrons accelerated in the inner EDR are then slowed down in the outer EDR, where the electron bulk kinetic energy transfers to magnetic energy (e.g., Zenitani et al. 2011). Moreover, we find that both $J_M E'_M$ and $J_L E'_L$ are negative in the outer EDR, implying that electrons were indeed decelerated in both the $\boldsymbol{L}$ and $\boldsymbol{M}$ directions. However, MMS1 and MMS2 detected a larger electron speed in the $\boldsymbol{L}$ direction than that recorded by MMS3 and MMS4 (Figure 3(c)), which is different from the previous simulations of antiparallel reconnection, which shows that the electron outflow is mainly decelerated in the $\boldsymbol{L}$ direction (Karimabadi et al. 2007). We suggest that electron flow v_{eM} was deflected to the $\boldsymbol{L}$ direction, leading to a larger v_{eL} in the outer EDR than in the inner EDR in this case.

It has been shown that the outer EDR, manifested as an outward-moving electron jet, may extend tens of the ion inertial lengths from the X-line (Phan et al. 2007; Shay et al. 2007), hence making the current sheet longer than tens of the ion inertial length, which is the expected scale that ions are fully coupled to reconnection (Mandt et al. 1994; Sharma et al. 2019). In this event, we do not know how long the outer EDR can be reached. Nevertheless, the elongation of the reconnecting current sheet due to the formation of the outer EDR may finally lead to the ion coupling in reconnection.

The outer EDR was first identified in kinetic simulations without a guide field, i.e., antiparallel geometry (Daughton et al. 2006; Fujimoto 2006; Karimabadi et al. 2007; Shay et al. 2007). It was later found that a small guide field could deflect the outer EDR away from the neutral plane or even destroy the outer EDR (Goldman et al. 2011; Zhou et al. 2014). Le et al. (2013) illustrate that the existence of the outer EDR and its property is largely controlled by the guide field strength and the inflow plasma β. However, the existence of the outer EDR in a large guide field regime (>1 B_0) has not been explored before. Our observations show that even with a guide field of more than 3 times the asymptotic reconnecting magnetic field, the outer EDR is formed and lies in the neutral plane, that is, without evident deflection. A

recent simulation with a large guide field or large plasma $\beta(\beta \gg 1)$ also found that the Hall magnetic field and the in-plane electron flow are symmetric in the inflow direction (Munoz et al. 2015; Sharma et al. 2019), substantially different from the reconnection with small to moderate guide field and small inflow plasma β, in which the Hall electromagnetic field and in-plane electron flow is asymmetric with respect to the neutral current sheet (Eastwood et al. 2010). In this event, the guide field is about 3.2 B_0, and the inflow $\beta \sim 1$. Therefore, more kinetic simulations are required to explore a broader parameter space. In addition, the collimated outer EDR and the symmetric Hall magnetic field in the large guide field/plasma β regime may have some intrinsic relationship and are worth further studying.

In summary, MMS simultaneously probed the inner and outer EDR of a secondary reconnection at the dayside magnetopause. We find that the outer EDR also exists in magnetic reconnection with a large guide field ($\sim$3.2 B_0). MMS simultaneously detected the oppositely directed electron jets, indicating that the MMS tetrahedron circumscribed the X-line. The spacecraft on the one side of the X-line observed the inner EDR, while the spacecraft on the other side of the X-line detected the outer EDR. Based on the fortuitous formation of the four MMS spacecraft, we estimate the maximum length of the inner EDR as 93 km $\sim$ 36 d_e. Considering that the EDR thickness was about 13.2 ± 3.8 km $\sim 5.1 \pm 1.5$ d_e, the lower bound of the dimensionless reconnection rate was estimated as 0.142 ± 0.041. This study provides a useful template for further investigating the structure of the EDR and estimating the reconnection rate in space plasma by employing multiple spacecraft observations.

Acknowledgments

We thank the entire Magnetospheric Multiscale (MMS) team for successful operation and the high-quality data. We acknowledge the use of NASA/GSFC's Space Physics Data Facility's OMNIWeb (or CDAWeb or ftp) Service. This work was supported by the National Natural Science Foundation of China (NSFC) under grants 41774154, 42074197, 42130211, and 42104156.

Data Availability

The data used in this study were obtained from the MMS Science Data Center (https://lasp.colorado.edu/mms/sdc/public/about/browse-wrapper/) and the OMNI website (https://spdf.gsfc.nasa.gov/pub/data/omni/omni_cdaweb/).

ORCID iDs

Z. C. Tian https://orcid.org/0000-0002-8251-8297
Z. H. Zhong https://orcid.org/0000-0003-0617-4418
D. J. Gershman https://orcid.org/0000-0003-1304-4769
Y. V. Khotyaintsev https://orcid.org/0000-0001-5550-3113
C. T. Russell https://orcid.org/0000-0003-1639-8298

References

Burch, J. L., Torbert, R. B., Phan, T. D., et al. 2016, Sci, 352, aaf2939
Chen, L. J., Hesse, M., Wang, S., et al. 2017, JGRA, 122, 5235
Daughton, W., Scudder, J., & Karimabadi, H. 2006, PhPl, 13, 072101
Deng, X. H., & Matsumoto, H. 2001, Natur, 410, 557
Eastwood, J. P., Shay, M. A., Phan, T. D., & Øieroset, M. 2010, PhRvL, 104, 205001
Ergun, R. E., Tucker, S., Westfall, J., et al. 2016, SSRv, 199, 167
Fujimoto, K. 2006, PhPl, 13, 072904
Goldman, M. V., Lapenta, G., Newman, D. L., Markidis, S., & Che, H. 2011, PhRvL, 107, 135
Hwang, K. J., Sibeck, D. G., Choi, E., et al. 2017, GeoRL, 44, 2049
Karimabadi, H., Daughton, W., & Scudder, J. 2007, GeoRL, 34, L13104
Karimabadi, H., Roytershteyn, V., Daughton, W., & Liu, Y.-H. 2013, SSRv, 178, 307
Le, A., Egedal, J., Ohia, O., et al. 2013, PhRvL, 110, 135004
Lin, J., Ko, Y., Sui, L., et al. 2005, ApJ, 622, 1251
Lindqvist, P. A., Olsson, G., Torbert, R. B., et al. 2016, SSRv, 199, 137
Liu, Y. H., Daughton, W., Karimabadi, H., Li, H., & Roytershteyn, V. 2013, PhRvL, 110, 265004
Liu, Y. H., Hesse, M., Guo, F., et al. 2017, PhRvL, 118, 085101
Mandt, M. E., Denton, R. E., & Drake, J. F. 1994, GeoRL, 21, 73
Munoz, P. A., Told, D., Kilian, P., Buchner, J., & Jenko, F. 2015, PhPl, 22, 082110
Phan, T. D., Drake, J. F., Shay, M. A., Mozer, F. S., & Eastwood, J. P. 2007, PhRvL, 99, 255002
Phan, T. D., Eastwood, J. P., Shay, M. A., et al. 2018, Natur, 557, 202
Pollock, C., Moore, T., Jacques, A., et al. 2016, SSRv, 199, 331
Priest, E., & Forbes, T. 2000, Magnetic Reconnection: MHD Theory and Applications (Cambridge: Cambridge Univ. Press)
Russell, C. T., Anderson, B. J., Baumjohann, W., et al. 2016, SSRv, 199, 189
Russell, C. T., Mellott, M. M., Smith, E. J., & King, J. H. 1983, JGR, 88, 4739
Scudder, J. D., Karimabadi, H., Daughton, W., & Roytershteyn, V. 2015, PhPl, 22, 303
Sharma, P. P., Shay, M. A., Phan, T. D., Matthaeus, W. H., & Chasapis, A. 2019, PhPl, 26, 082307
Shay, M. A., Drake, J. F., & Swisdak, M. 2007, PhRvL, 99, 155002
Shi, Q. Q., Shen, C., Dunlop, M. W., et al. 2006, GeoRL, 33, L08109
Sonnerup, B. U. O., & Scheible, M. 1998, in Analysis Methods for Multi-Spacecraft Data, ed. G. Paschmann & P. Daly (Noordwijk: ESA), 185
Swisdak, M. 2016, GeoRL, 43, 43
Torbert, R. B., Burch, J. L., Phan, T. D., et al. 2018, Sci, 362, 1391
Vasyliunas, V. M. 1975, RvGSP, 13, 303
Xiao, C. J., Pu, Z. Y., Wang, X. G., et al. 2007, GeoRL, 34, L01101
Zenitani, S., Hesse, M., Klimas, A., & Kuznetsova, M. 2011, PhRvL, 106, 195003
Zhong, Z. H., Zhou, M., Liu, Y. H., et al. 2022, ApJL, 926, L27
Zhong, Z. H., Zhou, M., Tang, R. X., et al. 2020, ApJL, 892, L5
Zhou, M., Deng, X. H., Tang, R. X., et al. 2014, JGRA, 119, 1541
Zhou, M., Deng, X. H., Zhong, Z. H., Pang, Y., & Lindqvist, P. A. 2019, ApJ, 870, 34
Zhou, M., Zhong, Z. H., & Deng, X. H. 2022, RvMPP, 6, 15